Macromolecular Materials and Engineering
Open Access
www.mame-journal.de

Check for updates

Thermo-Responsive Ultrafiltration Block Copolymer Membranes Based on Polystyrene-*block*-poly(diethyl acrylamide)

*Florian V. Frieß, Frank Hartmann, Lea Gemmer, Jens Pieschel, Bart-Jan Niebuur, Matthias Faust, Tobias Kraus, Volker Presser, and Markus Gallei**

Within the present work, a thermo-responsive ultrafiltration membrane is manufactured based on a polystyrene-*block*-poly(diethyl acrylamide) block copolymer (BCP). The poly(diethyl acrylamide) block segment features a lower critical solution temperature (LCST) in water, similar to the well-known poly(*N*-isopropylacrylamide), but having increased biocompatibility and without exhibiting a hysteresis of the thermally induced switching behavior. The BCP is synthesized via sequential "living" anionic polymerization protocols and analyzed by ^{1}H-NMR spectroscopy, size exclusion chromatography, and differential scanning calorimetry. The resulting morphology in the bulk state is investigated by transmission electron microscopy (TEM) and small-angle X-ray scattering (SAXS) revealing the intended hexagonal cylindrical morphology. The BCPs form micelles in a binary mixture of tetrahydrofuran and dimethylformamide, where BCP composition and solvent affinities are discussed in light of the expected structure of these micelles and the resulting BCP membrane formation. The membranes are manufactured using the non-solvent induced phase separation (NIPS) process and are characterized via scanning electron microscopy (SEM) and water permeation measurements. The latter are carried out at room temperature and at 50 °C revealing up to a 23-fold increase of the permeance, when crossing the LCST of the poly(diethyl acrylamide) block segment in water.

1. Introduction

Smart polymers open a way to introduce new exciting aspects and possibilities in conventional materials.[1] Within this context, stimuli-responsive polymers can react to changes in their environment, for example, temperature, pH value, or other triggers, with changes in their macromolecular properties.[1–7] One possibility to achieve a thermally induced response focuses on a lower critical solution temperature (LCST) or an upper critical solution temperature (UCST) in a specific medium.[8–11] The different solubility of the polymer chains at different temperatures can be exploited to use, for example, polymer micelles to act as carriers for specific cargo compounds. In this manner APPOLD et al. were able to design a block copolymer (BCP) of poly(*N,N*-dimethylaminoethyl methacrylate) and poly(methyl methacrylate)-*co*-poly(*N,N*-dimethyl aminoethyl methacrylate) to encapsulate a polypyridyl ruthenium complex and release it through applying ultrasound or temperature.[12] Besides this example there are numerous other

F. V. Frieß, F. Hartmann, L. Gemmer, J. Pieschel, M. Gallei
Polymer Chemistry
Saarland University
66123 Saarbrücken, Germany
E-mail: markus.gallei@uni-saarland.de
V. Presser, M. Gallei
Saarene
Saarland Center for Energy Materials and Sustainability
Campus C4 2, 66123 Saarbrücken, Germany

B.-J. Niebuur, T. Kraus
INM – Leibniz Institute for New Materials
66123 Saarbrücken, Germany
M. Faust
Institute for Physical Process Technology
Saarland University of Applied Sciences
Göbenstr. 40, 66117 Saarbrücken, Germany
T. Kraus
Colloid and Interface Chemistry
Saarland University
66123 Saarbrücken, Germany
V. Presser
Department of Materials Science and Engineering
Saarland University
66123 Saarbrücken, Germany
V. Presser
INM – Leibniz Institute for New Materials
Campus D2 2, 66123 Saarbrücken, Germany

The ORCID identification number(s) for the author(s) of this article can be found under https://doi.org/10.1002/mame.202300113

© 2023 The Authors. Macromolecular Materials and Engineering published by Wiley-VCH GmbH. This is an open access article under the terms of the Creative Commons Attribution License, which permits use, distribution and reproduction in any medium, provided the original work is properly cited.

DOI: 10.1002/mame.202300113

stimuli-responsive BCP micelles, which are mainly investigated in the field of drug delivery.[13,14] The mechanism of the changes in the polymer chains around the LCST was investigated by KOLBERG et al. and found to be a cooperative effect of different chains together.[15] Furthermore, this change in solubility, or more precisely, in the chain conformation can also be used for modulating porous materials leading to a change of permeation characteristics upon applying external triggers. This feature can then be used to design polymer membranes, switchable by the permeate or other internal or external triggers. Within this context, porous membranes can be divided into two classes: On the one hand, some authors modify existing membranes, like FROST et al., who functionalized a track-etched poly(ethylene terephthalate) ultrafiltration membrane with poly(*N*-isopropylacrylamide) (PNIPAM) via surface-initiated atom-transfer radical polymerization (SI-ATRP). The authors showed a temperature switchable rejection of silica nanoparticles for their membranes.[16] In another example, TRIPATHI et al. functionalized commercial micro-filtration membranes with PNIPAM via a polydopamine linker and were able to show thermo-responsive behavior in both water permeance and protein rejection.[17] On the other hand, there are some solutions that utilize the intrinsic properties of the polymers used to manufacture the membrane. For example, SCHACHER et al. used polystyrene-*block*-poly(*N,N*-dimethyl aminoethyl methacrylate) BCPs to manufacture ultrafiltration membranes, which exhibited temperature-dependent exclusion of silica nanoparticles.[18] Moreover, CETINTAS et al. used PS-*b*-PNIPAM BCPs synthesized via reversible addition-fragmentation polymerization to fabricate polymer membranes, and were able to show a permeability increase of almost 400% by raising the temperature from 20 to 50 °C.[19] Lastly, there is also the possibility of using a polymer blend in the membrane formation step, as shown by CAI et al., who used a blend of polyvinylidene fluoride (PVDF) and palygorskite-*g*-PNIPAM in a combination of immersion precipitation and thermally induced phase separation process. They enhanced the hydrophilicity compared to neat PVDF membranes, and thermo-responsivity was introduced.[20] One of the most common polymers featuring an LCST behavior is PNIPAM, while its derivative poly(diethyl acrylamide) (PDEAAm) is investigated much less in the polymer membrane field. In general, both polymers feature a similar LCST in the range of just above 30 °C.[21,22] While PNIPAM features a very sharp transition at the LCST, the transition of PDEAAm is much more distributed over a larger temperature interval.[23] On a more macroscopic scale, the phase transition enthalpy is found to be lower for PDEAAm than for PNIPAM that is said to point to a different water structure surrounding the polymers.[22] While this may be a disadvantage for PDEAAm, the transition of this polymer occurs at the same region for heating and cooling, while PNIPAM shows hysteresis.[23,24] Another advantage of PDEAAm is its better biocompatibility compared to PNIPAM,[25,26] which is important for potential biomedical applications.

Regarding the polymer synthesis, DEAAm is an alkyl acrylate derivative, and there are some special precautions necessary to suppress side reactions of the labile α-hydrogen during living anionic polymerization.[27] To stabilize the living chain-end, the electron density distribution of the metal ester enolate ion pair has to be influenced by an aggregation equilibrium enabling a controlled polymer growth.[28] Most commonly, different Lewis acids are used in order to facilitate this equilibrium. ISHIZONE et al. combined the Lewis acid character of dialkylzinc with its multivalent coordination to stabilize the active chain-end in tetrahydrofuran (THF).[29] The polymerization of acrylamides was also tested with diethylzinc as an additive. KOBAYASHI et al. found that the coordination of the active chain-end slowed down the propagation, so the temperature needed to be raised to 0 °C. As a side effect, the coordination of the active chain-end with diethylzinc also leads to a highly isotactic polymer, which is insoluble in THF.[30] In comparison, ANDRÉ et al. found that the usage of triethylaluminium leads to heterotactic DEAAm, but triethylaluminium can also initiate the polymerization.[31] When triethyl borane (BEt_3) was used by KOBAYASHI et al. instead, the resulting polymer showed syndiotactic triads. BEt_3 also coordinates stronger to the active chain-end and could be used in a lower excess to obtain polymers with low dispersity.[32] By the amount of added Lewis acid and block copolymerization, the solubility of DEAAm can be adjusted.[32,33]

In this work, polystyrene-*block*-poly(diethyl acrylamide) (PS-*b*-PDEAAm) is synthesized with varying chain lengths, and thermo-responsive block copolymer membranes are fabricated using the non-solvent induced phase-inversion process. These membranes are characterized using scanning electron microscopy and water permeation measurements at room temperature and above the LCST.

2. Results and Discussion

2.1. Polymer Synthesis

The BCP PS-*b*-PDEAAm **P2** was synthesized via sequential anionic polymerization, as shown in **Scheme 1**. In the first step, styrene **1** was polymerized in THF at −78 °C for 1 h, after initiation with *sec*-butyl lithium. The active polymer chains were functionalized with diphenyl ethylene to obtain **P1DPHLi**, to provide a steric hinderance to suppress side-reactions with the DEAAm carbonyl moiety in the following synthesis step. DEAAm **2** was polymerized for 16 h at 0 °C with the help of triethyl borane as Lewis acid, which forms a complex with the active chain ends leading to structural control.[32]

The analytical data in **Table 1** compile the obtained molecular weight of the resulting BCPs PS-*b*-PDEAAm after sequential block copolymerization of the respective monomers.

The first block of the BCPs, PS, was measured using SEC against a PS standard calibration. Therefore, the resulting molecular weights can be directly compared based on the same solution behavior. The dispersity index values of the three PS blocks were determined at below 1.05, as expected for good control over the reaction using living carbanionic polymerization. After end-functionalization with DPE and the addition of BEt_3, DEAAm was polymerized in a subsequent step at 0 °C. The resulting BCPs were analyzed via SEC (**Figure 1**) with dimethyl formamide with LiBr as a salt additive. Determining the molar masses of the amphiphilic BCPs by SEC was performed versus PMMA standards. Therefore, the absolute value of the M_n determined this way is not representative of the BCP. However, since the molecular masses for the first block segment (PS), determined by SEC, can be considered absolute, the molecular mass of the

 © 2023 The Authors. Macromolecular Materials and Engineering published by Wiley-VCH GmbH

14392054, 2023, 11, Downloaded from https://onlinelibrary.wiley.com/doi/10.1002/mame.202300113 by Universitaet Des Saarlandes, Wiley Online Library on [31/01/2024]. See the Terms and Conditions (https://onlinelibrary.wiley.com/terms-and-conditions) on Wiley Online Library for rules of use; OA articles are governed by the applicable Creative Commons License

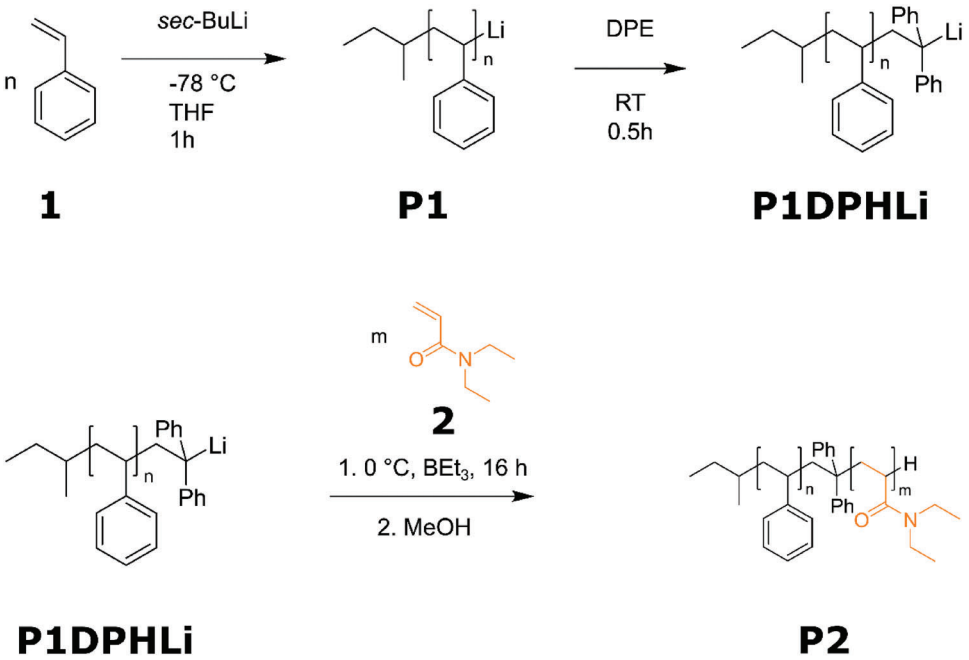

Scheme 1. Reaction scheme for the sequential anionic polymerization of the monomers styrene and diethyl acrylamide leading to the BCP polystyrene-*block*-poly(diethyl acrylamide) P2 (PS-*b*-PDEAAm). In the first step styrene is initiated by *sec*-Butyllithium in THF at −78 °C. After 1 h, the active chain ends are functionalized with diphenyl ethylene at room temperature. Following, the reaction mixture is cooled to 0 °C, and triethyl borane and diethyl acrylamide are added and polymerized for 16 h.

Table 1. Analytical data of the block copolymerization of PS-*b*-PDEAAm in THF with BEt_3.

Polymer	M_n [PS][a] [kg mol^{-1}]	M_n [BCP][b] [kg mol^{-1}]	$Đ$[b]	M_n [BCP][c] [kg mol^{-1}]	w [PDEAAm][c] [wt.%]
PS_{70}-*b*-$PDEAAm_{17}$	70.2	71.5	1.11	87.4	23.5
PS_{125}-*b*-$PDEAAm_{43}$	125	118	1.16	168	25.6
PS_{131}-*b*-$PDEAAm_{42}$	131	139	1.22	173	24.3

[a] SEC in THF versus PS [b] SEC in DMF +1 g L^{-1} LiBr at 60°C versus PMMA [c] determined by ^{1}H-NMR spectroscopy in $CDCl_3$

BCP can be calculated from these and the composition, extracted from the ^{1}H-NMR measurements. As a conclusion from the SEC measurements, the resulting dispersity indices were elevated compared to the aforementioned THF system, resulting in a dispersity index value of 1.1 for the first PS block. This broadening of the DMF SEC system also led to the dispersity of 1.11 to 1.22 for the BCP. The molecular weight distributions of the BCPs from Table 1 are given in Figure 1d. A slight broadening of the molecular weight distribution was observed for polymer PS_{125}-*b*-$PDEAAm_{43}$ and PS_{131}-*b*-$PDEAAm_{42}$. The absolute molecular weights of the BCPs were determined using the molecular weights from the PS block in combination with the amounts of PDEAAm, as determined by ^{1}H-NMR spectroscopy, shown in Figure 1a. The ^{1}H-NMR spectra showed a similar PDEAAm content for all three BCPs ranging from 24.5 to 25.6 wt.% (Section S1.1, Figures S1–S3, Supporting Information). Investigations of the glass transition temperature (T_g) via differential scanning calorimetry (DSC) were performed, and the T_g for the PS homopolymer showed a value of 106.8 °C, which is within the expected range.[34] However, an additionally prepared PDEAAm homopolymer of similar M_n (Section S1.2, Supporting Information) to the PDEAAm blocks in the BCP revealed a T_g of 94.5 °C, hence similar to the PS block segment. As the two block segments of the BCP have similar T_g, there was no indication of microphase separation in these investigations. Thermograms of all BCP are provided in (Section S1.3, Figure S4, Supporting Information).

2.2. Bulk Morphologies

To verify if the synthesized BCPs feature a microphase separation capability, the bulk morphology was analyzed via transmission electron microscopy (TEM) and small-angle X-ray scattering (SAXS). For this purpose, BCP films were prepared by solvent annealing from chloroform and a subsequent temperature annealing at 130 °C for at least 3 days. Thin slices were prepared via ultramicrotomy, followed by staining with RuO_4 to enhance the electron contrast in TEM. The first polymer, PS_{70}-*b*-$PDEAAm_{17}$, (**Figure 2**a) shows light PDEAAm hexagonally packed cylinders in a darker appearing stained PS matrix. The observed cylinders were of a size of 39.3 ± 4.4 nm and were not very well ordered over larger length scales. The corresponding SAXS measurement (Figure 2d) showed a strong primary peak at q_0 = 0.0171 Å^{-1}

© 2023 The Authors. Macromolecular Materials and Engineering published by Wiley-VCH GmbH

14392054, 2023, 11, Downloaded from https://onlinelibrary.wiley.com/doi/10.1002/mame.202300113 by Universitaet Des Saarlandes, Wiley Online Library on [31/01/2024]. See the Terms and Conditions (https://onlinelibrary.wiley.com/terms-and-conditions) on Wiley Online Library for rules of use; OA articles are governed by the applicable Creative Commons License

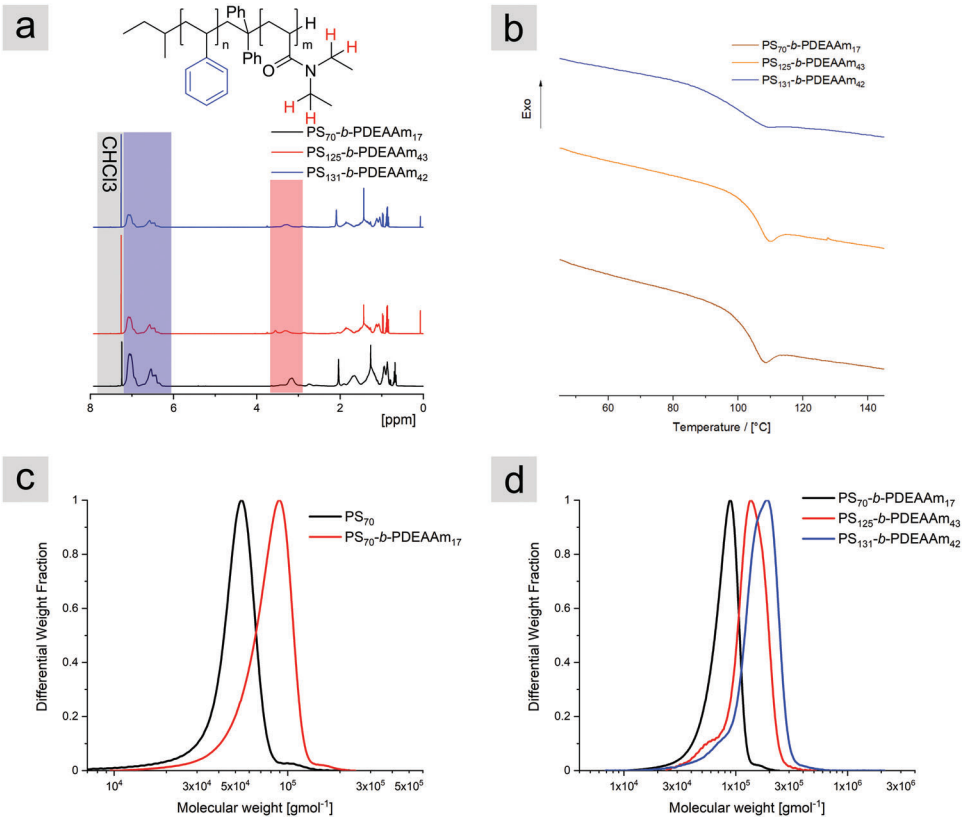

Figure 1. a) ^{1}H-NMR-spectra of PS-*b*-PDEAAm, measured at 400 MHz and 300 K in $CDCl_3$ b) Thermograms of homopolymers PS and PDEAAM, and the respective BCP PS-*b*-PDEAAm measured at 10 K min^{-1} in N_2 atmosphere c) Molecular weight distributions of the PS_{70} block (in black) of PS_{70}-*b*-$PDEAAm_{17}$ (in red), measured in DMF against PMMA standard d) Molecular weight distributions of polymers PS-*b*-PDEAAm, measured in DMF against PMMA standard.

and secondary Bragg reflections at $\sqrt{3} \times q_0$ and $\sqrt{7} \times q_0$, expected for hexagonally packed cylinders[35] with a repeat distance of $2\pi/q_0 = 36.7$ nm, which is in good agreement with the result from TEM. The low intensities of the secondary Bragg peaks confirm the weak long-range order of the structure. By enlarging the BCP from 87.4 to 168 kg mol^{-1} the mass ratio of PDEAAm was also slightly increased from 23.5 to 25.6 wt.%. The resulting TEM images (Figure 2b) of the bulk morphology revealed a weakly ordered structure without recognizable pattern. The SAXS pattern (Figure 2e) showed a primary Bragg peak at $q_0 = 0.0171$ Å^{-1}, which corresponds to a repeat distance of $2\pi/q_0 = 58.2$ nm. Furthermore, a very broad secondary peak at ≈0.025 Å^{-1} was present, which could not be assigned to a classical ordered phase. As attempts to stain polymer PS_{131}-*b*-$PDEAAm_{42}$ with RuO_4 failed, the investigation of this BCP morphology was performed with iodine as a staining agent instead of RuO_4. In this case the PDEAAm phase should appear darker, and therefore dark PDEAAm cylinders should be visible in a light PS matrix. Indeed, the expected hexagonally packed cylindrical morphology for the mass ratio of 24.3 wt.% could be observed in the corresponding TEM image in Figure 2c. The morphology appeared to be larger (64.9 ± 8.7 nm) compared to Figure 2a for a polymer with a similar mass ratio of PDEAAm but just about half of the total molecular weight. The primary Bragg reflection from SAXS (Figure 2f) confirms the increased repeat distance of $2\pi/q_0 = 80.6$ nm. The weak secondary Bragg peaks are found at $\sqrt{3} \times q_0$ and $\sqrt{7} \times q_0$, which again corresponds to a hexagonally packed phase and confirms the structure observed in the TEM images. The secondary Bragg peaks are always very weak and have a broad maximum, so a lamellar ordering with a ratio of $2 \times q_0$ and $3 \times q_0$ cannot be excluded. Overall, the weak ordering of the morphology in polymers PS_{70}-*b*-$PDEAAm_{17}$ and PS_{131}-*b*-$PDEAAm_{42}$ as well as the unclear phase separation in polymer PS_{125}-*b*-$PDEAAm_{43}$ are a hint for a border area of two different BCP morphologies. The expected morphology is usually estimated from the volume ratio of the different polymer blocks through the mean-field phase diagram.[36] The required density of PDEAAm and interaction parameters for this system have not been reported yet.

2.3. Micelle Formation of PS_{125}-*b*-$PDEAAm_{43}$ BCPs

The micellization behavior of PS_{125}-*b*-$PDEAAm_{43}$ prior to the membrane formation was examined in a binary solvent mixture of DMF and THF, which was considered a good solvent mixture for micelle formation and the intended SNIPS process. In this mixture, THF is a better solvent for the PS block and DMF is better for the PDEAAm block, as can be concluded by comparing

© 2023 The Authors. Macromolecular Materials and Engineering published by Wiley-VCH GmbH

14392054, 2023, 11, Downloaded from https://onlinelibrary.wiley.com/doi/10.1002/mame.202300113 by Universitaet Des Saarlandes, Wiley Online Library on [31/01/2024]. See the Terms and Conditions (https://onlinelibrary.wiley.com/terms-and-conditions) on Wiley Online Library for rules of use; OA articles are governed by the applicable Creative Commons License

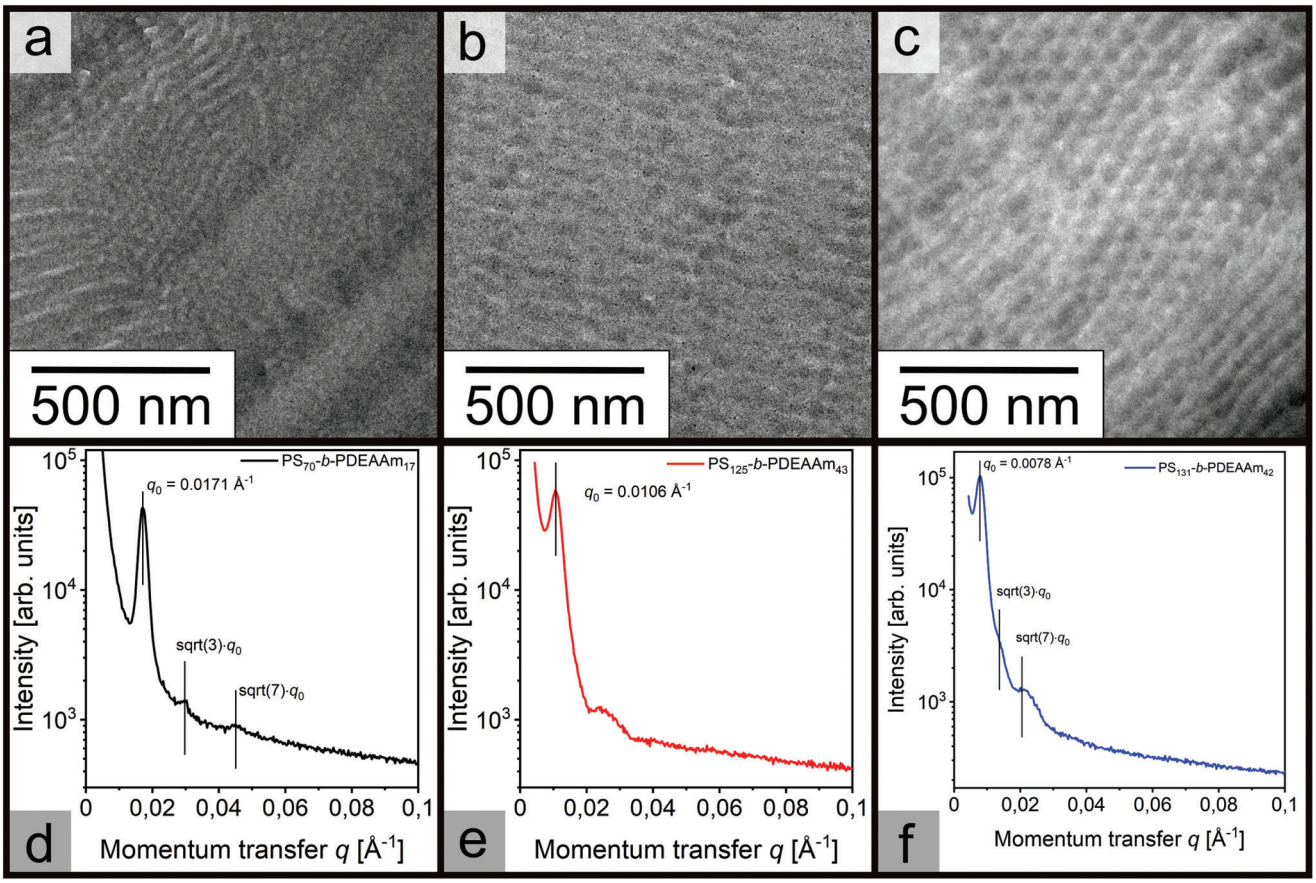

Figure 2. a) Transmission electron micrograph of an ultra-thin slice of PS_{70}-*b*-$PDEAAm_{17}$, stained with RuO_4 b) Transmission electron micrograph of an ultra-thin slice of PS_{125}-*b*-$PDEAAm_{43}$, stained with RuO_4 c) Transmission electron micrograph of an ultra-thin slice of PS_{131}-*b*-$PDEAAm_{42}$, stained with I_2 d–f) SAXS analysis of the corresponding BCPs.

Table 2. Hildebrandt and Hansen parameters of the relevant solvents and polymers.

Polymer/solvent	δ_d [$MPa^{1/2}$]	δ_p [$MPa^{1/2}$]	δ_h [$MPa^{1/2}$]	δ_D [$MPa^{1/2}$]
PS[38]	18.1 ± 0.1	1.9 ± 0.1	2.8 ± 0.1	18.4 ± 0.1
PDEAAm[39]	17.9	1.78	11.5	21.4
DMF[37]	17.4	13.7	11.3	24.8
THF[37]	16.8	5.7	8.0	18.6
THF/DMF (2:3 wt.%)	17.1	10.3	9.9	22.3

the experimentally determined Hildebrandt and Hansen parameters presented in **Table 2**. The overall value for the binary solvent mixture can then be calculated from the values of THF and DMF, weighted with their weight fraction and density.[37]

Based on these parameters, micelles were expected to form with a core of the PS block and a corona of PDEAAm, since the solvent mixture overall fits more closely to the latter. In **Figure 3**, the resulting polymer micelles are shown, as determined from TEM investigations, using a diluted mixture of ≈0.002 mg mL^{-1} polymer PS_{125}-*b*-$PDEAAm_{43}$ with THF and DMF (2:3 by weight).

As can be concluded from these investigations, BCP micelles were observed with a diameter of 45 ± 6 nm ($N = 25$).

2.4. Membrane Characterization

Polymer membranes were fabricated from all three synthesized BCPs. To this end a polymer solution consisting of the binary solvent mixture of THF and DMF (2:3 by weight) and a solid content of ≈25 to 30 wt.% was prepared. This polymer solution was then cast on a polyester support and precipitated in water after defined evaporation times after doctor-blading. Based on the results of the micellization experiments, as well as the microphase separation investigation and the Hansen parameters, a NIPS mechanism during the membrane formation was plausible. Moreover, as the THF evaporated after casting the BCP solution, the solvent mixture became more favorable toward PDEAAm and a more dilute phase, featuring predominantly PDEAAm, and a more concentrated phase, featuring predominantly PS was expected. Generally, the more concentrated phase forms the matrix of the BCP membrane and the more dilute phase the pores.[40] The membranes were therefore expected to form a polystyrene matrix upon evaporation of THF, with the PDEAAm being on the inside of the

© 2023 The Authors. Macromolecular Materials and Engineering published by Wiley-VCH GmbH

14392054, 2023, 11, Downloaded from https://onlinelibrary.wiley.com/doi/10.1002/mame.202300113 by Universitaet Des Saarlandes, Wiley Online Library on [31/01/2024]. See the Terms and Conditions (https://onlinelibrary.wiley.com/terms-and-conditions) on Wiley Online Library for rules of use; OA articles are governed by the applicable Creative Commons License

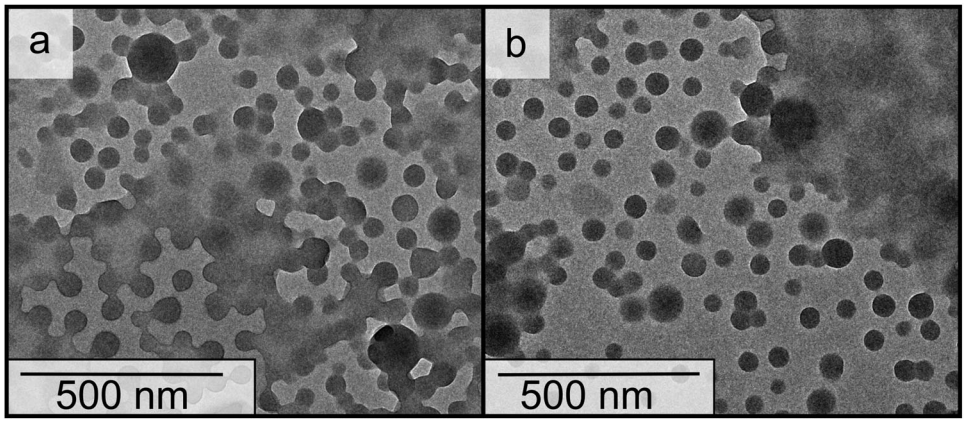

Figure 3. Transmission electron micrograph of a micellar solution (0.002 mg mL^{-1}) of PS_{125}-b-$PDEAAm_{43}$ prepared in a THF/DMF (2:3 by weight) solvent mixture, both a,b) are from the same solution but from different regions of the sample.

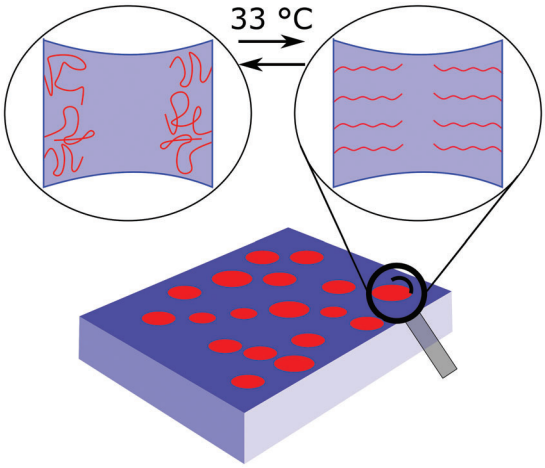

Figure 4. Schematic view of the proposed membrane structure with a polystyrene matrix (blue) and PDEAAm (red) lined pores.

membrane pores. This is shown schematically in **Figure 4**. When heating the membrane above the LCST of PDEAAm in water or using hot water (above the LCST of 33 °C) within the filtration experiment, the PDEAAm chains, which were swollen below that temperature, are expected to collapse,[41,42] creating a larger pore volume and higher permeation.

First, the polymer PS_{70}-*b*-$PDEAAm_{17}$ was dissolved in the binary mixture of THF and DMF (2:3 by weight). From this viscous solution with a solid content of 31%, a polymer film was cast with a doctor blade with a blade gap of 200 µm on a polyester nonwoven. After an evaporation time of 15 s (polymer PS_{70}-*b*-$PDEAAm_{17}$ and PS_{125}-*b*-$PDEAAm_{43)}$, or 10 s (polymer PS_{131}-*b*-$PDEAAm_{42}$) the polymer film was precipitated in water. The variation of the evaporation times was chosen because of the membrane structure observed after 15 s for PS_{131}-*b*-$PDEAAm_{42}$, where almost no pores were observed (Figure S5, Supporting Information). As can be concluded from **Figure 5** the resulting membrane features regions of good pore formations (Figure 5a) and regions of poor pore formation with large areas without pores (Figure 5b).

Since the PDEAAm block exhibits an LCST in water and is soluble below this temperature, it was assumed that the precipitation step could be an issue, since the water of the precipitation bath was at room temperature. With this in mind, the membranes were precipitated in water baths at 40 °C. In **Figure 6**, the typical surface of the membranes is shown on the left-hand side, while cross-sections of the membranes are shown on the right-hand side.

The membrane of PS_{70}-*b*-$PDEAAm_{17}$ shown in Figure 6a,b exhibited a porous structure with a diameter of 22 ± 6 nm and a sponge-like sub-structure typical for NIPS membranes.[43] The PS_{125}-*b*-$PDEAAm_{43}$ membrane structure shown in (c,d) was very similar to the first membrane, featuring a pore diameter of 36 ± 8 nm. This increased pore diameter, which also seemed present in the sponge-like substructure, was attributed to the increase in molecular weight from polymer PS_{70}-*b*-$PDEAAm_{17}$ to PS_{125}-*b*-$PDEAAm_{43}$. This molecular weight and pore size dependency was previously found for BCPs of polystyrene and poly(4-vinylpyridine).[44] In contrast, the membrane of polymer PS_{131}-*b*-$PDEAAm_{42}$, shown in Figure 6e,f featured a relatively dense surface with very large and ill-defined pores. Nevertheless, all membranes were subjected to thermo-responsive ultrafiltration experiments in the subsequent section to gain further insights into the switching capability.

2.5. Characterization of the Thermo-Responsive Properties of the NIPS Membranes

To investigate the thermo-responsive behavior of the block copolymer membranes the water permeation was determined via a dead-end filtration cell. The measurements were carried out at room temperature (RT) and 50 °C, i.e., well above the LCST of the PDEAAm block.[22] In **Table 3** the mean values are summarized. The values for measurements at 50 °C are corrected for the viscosity change of water (as shown in the Equation S4, Supporting Information).

At first, the different water permeation at room temperature directly correlated with the pore diameters found within the SEM images of the BCP membranes, shown in Figure 5. From PS_{70}-*b*-$PDEAAm_{17}$ to PS_{125}-*b*-$PDEAAm_{43}$ the average diameter increased by roughly 50 %, and the membrane of PS_{131}-*b*-$PDEAAm_{42}$ exhibited an irregular surface without well-defined

 © 2023 The Authors. Macromolecular Materials and Engineering published by Wiley-VCH GmbH

14392054, 2023, 11, Downloaded from https://onlinelibrary.wiley.com/doi/10.1002/mame.202300113 by Universitaet Des Saarlandes, Wiley Online Library on [31/01/2024]. See the Terms and Conditions (https://onlinelibrary.wiley.com/terms-and-conditions) on Wiley Online Library for rules of use; OA articles are governed by the applicable Creative Commons License

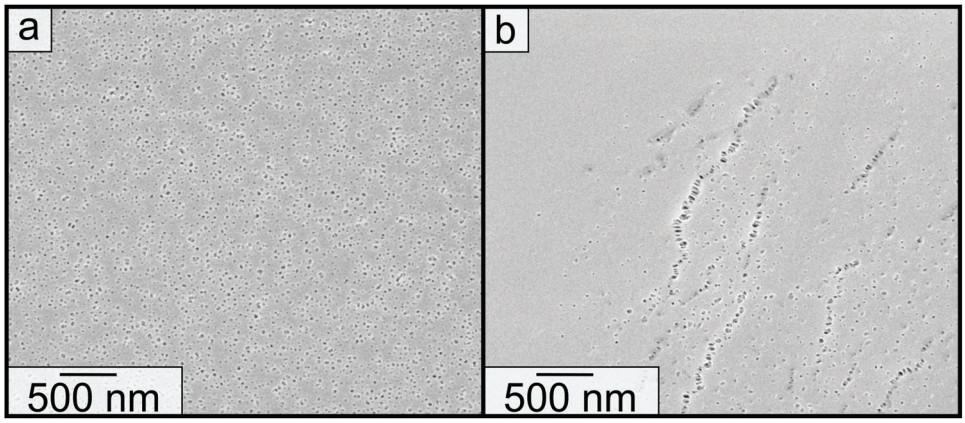

Figure 5. Scanning electron micrographs of the membranes from polymer PS_{70}-*b*-$PDEAAm_{17}$ precipitated at room temperature. a) Area with good pore distribution b) Area of poor pore formation.

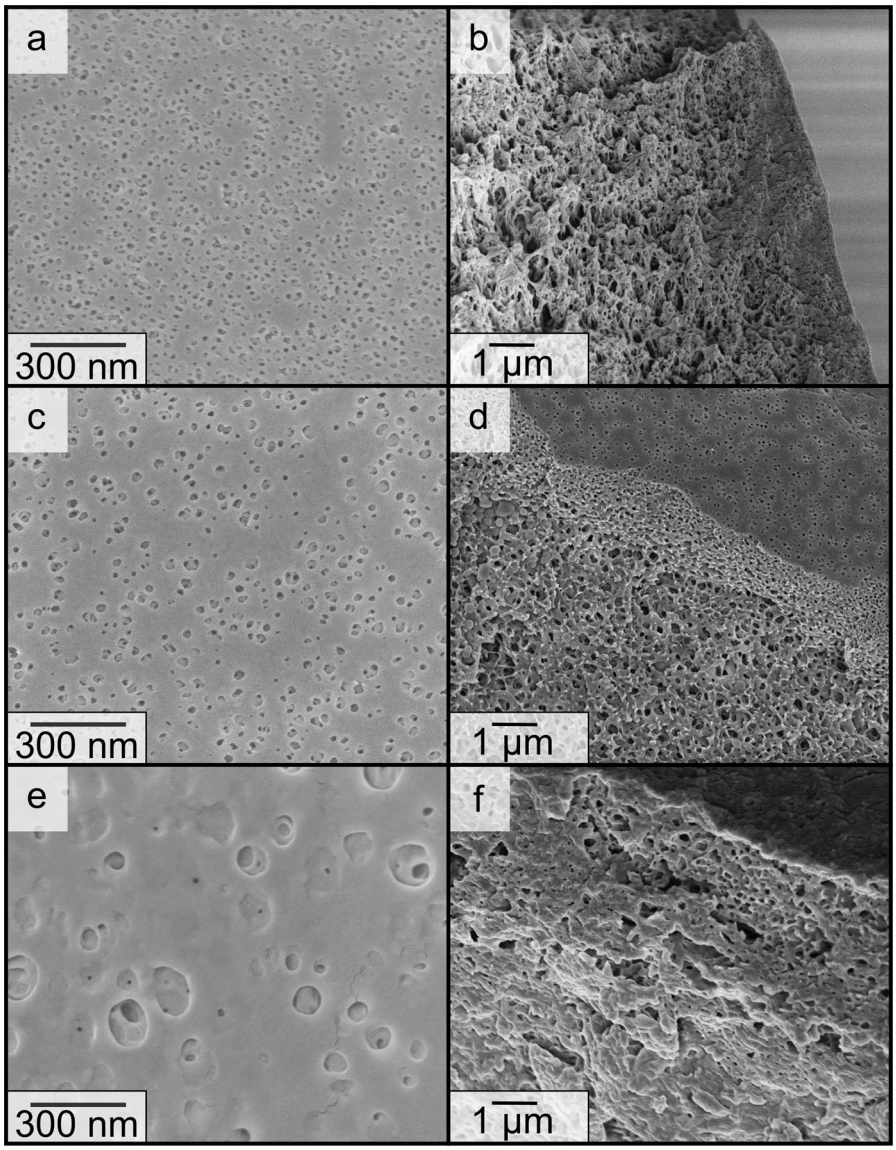

Figure 6. Scanning electron micrographs of the membrane surface and cross-section of the membranes of a,b) PS_{70}-b-$PDEAAm_{17}$, c,d) PS_{125}-b-$PDEAAm_{43}$ with 15 s evaporation time, and e,f) PS_{131}-b-$PDEAAm_{42}$ with 10 s evaporation time.

 © 2023 The Authors. Macromolecular Materials and Engineering published by Wiley-VCH GmbH

14392054, 2023, 11, Downloaded from https://onlinelibrary.wiley.com/doi/10.1002/mame.202300113 by Universitaet Des Saarlandes, Wiley Online Library on [31/01/2024]. See the Terms and Conditions (https://onlinelibrary.wiley.com/terms-and-conditions) on Wiley Online Library for rules of use; OA articles are governed by the applicable Creative Commons License

Table 3. Summary of the means of the water permeation for the three PS-*b*-PDEAAm block copolymer membranes, measured at room temperature and 50 °C as well as at room temperature after 50 °C. The water permeation values at 50 °C are corrected for the viscosity change of water, as shown in the experimental section.

Membrane	RT	50 °C [corr.]	$RT_{after\ 50\ °C}$
	[$Lbar^{-1}\ h^{-1}\ m^{-2}$]	[$Lbar^{-1}\ h^{-1}\ m^{-2}$]	[$Lbar^{-1}\ h^{-1}\ m^{-2}$]
PS_{70}-*b*-$PDEAAm_{17}$	25	590	77
PS_{125}-*b*-$PDEAAm_{43}$	512	757	395
PS_{131}-*b*-$PDEAAm_{42}$	48	261	118

pores. Therefore, the obtained values were within the expected range. When comparing the change in water permeation from RT to 50 °C there was a 23-fold increase of the water permeation for the membrane PS_{70}-*b*-$PDEAAm_{17}$, whereas the increase for PS_{125}-*b*-$PDEAAm_{43}$ and PS_{131}-*b*-$PDEAAm_{42}$ was found to be much smaller. This behavior could be attributed to the average pore size, as obtained from the SEM images in Figure 6. As the increase in water permeation is facilitated via the collapse of the PDEAAm chains, illustrated in Figure 4, the relative change of diameter of the smaller pores could be larger than for the larger pores. Finally, the permeation at room temperature and after the membrane was exposed to 50 °C showed a value in the same range as before. For membranes of PS_{70}-*b*-$PDEAAm_{17}$ and PS_{131}-*b*-$PDEAAm_{42}$ the permeation stays higher and for PS_{125}-*b*-$PDEAAm_{43}$ the permeation is decreased, compared to the first measurements at room temperature. This observation could be corroborated by findings from the scanning electron micrographs taken after the permeation measurements, as shown in **Figure 8**. The surface of PS_{70}-*b*-$PDEAAm_{17}$ shows no discernable change, and the pore diameter stayed unchanged within the error limits. In contrast, the BCP membrane obtained from PS_{125}-*b*-$PDEAAm_{43}$ showed a membrane surface significantly changed with fewer pores, which can explain the decreased permeation for this sample.

For a better understanding of these changes in the membrane performance when crossing the LCST of PDEAAm, the water permeation for the membrane cast from PS_{70}-*b*-$PDEAAm_{17}$ was monitored over a longer period of time. In **Figure 7b** the course of the water permeation is shown in dependence on time. Porous polymer membranes are expected to be compressed by the applied water pressure and therefore exhibit a decreasing permeation at constant pressure, when exposed over long periods. A higher porosity leads to more compression and therefore a lower permeation, as shown by PERSSON et al.[45] Figure 7b) shows the higher porosity at elevated temperatures. This higher porosity is easily explained by the collapse of the PDEAAm chains throughout the membrane. It shows the addressability of the LCST within the whole membrane in contrast to being a surface phenomenon. Analogously, this chain collapse could explain the loss of surface structure during the measurement at 50°C in the membrane of PS_{125}-*b*-$PDEAAm_{43}$. The larger pores on the surface and cross-section, could collapse partially or fully when the pressure is applied while the PDEAAm chains are in the collapsed state (Figure 6).

3. Conclusion

To summarize, we were able to polymerize styrene and diethyl acrylamide via sequential anionic polymerization, utilizing diphenylethylene as a steric mediator, as well as triethyl borane as Lewis acid functioning as a complexing agent during the polymerization of DEAAm. These block copolymers were characterized via SEC, ^{1}H-NMR spectroscopy, and DSC. Three block copolymers with molecular weights of 87.4 to 173 kg mol^{-1} were obtained. The microphase separation in the bulk state was investigated by TEM and SAXS on thin film slices. For the polymers PS_{70}-*b*-$PDEAAm_{17}$ and PS_{131}-*b*-$PDEAAm_{42}$ a hexagonal cylindrical morphology was found, while for polymer PS_{125}-*b*-$PDEAAm_{43}$ only disordered structures could be elucidated. Following, the micellization of the block copolymers was investigated in a

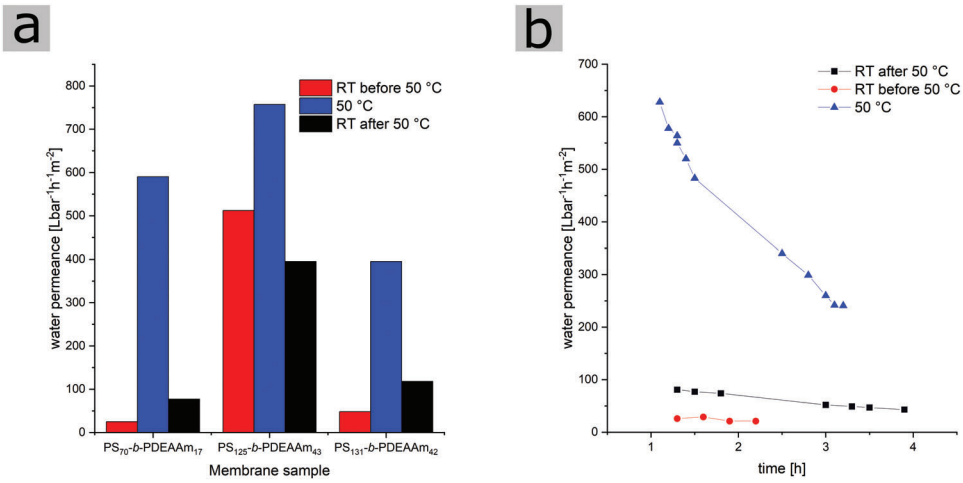

Figure 7. a) Bar diagram of the mean values of the water permeation, showing the values for room temperature, 50 °C and room temperature again after the measurement at elevated temperature, measured at 1 bar trans membrane pressure. b) Water permeation evolution of the membrane of P1 in dependence of time, after an equilibration period of 1 h, measured at 1 bar trans membrane pressure.

 © 2023 The Authors. Macromolecular Materials and Engineering published by Wiley-VCH GmbH

14392054, 2023, 11, Downloaded from https://onlinelibrary.wiley.com/doi/10.1002/mame.202300113 by Universitaet Des Saarlandes, Wiley Online Library on [31/01/2024]. See the Terms and Conditions (https://onlinelibrary.wiley.com/terms-and-conditions) on Wiley Online Library for rules of use; OA articles are governed by the applicable Creative Commons License

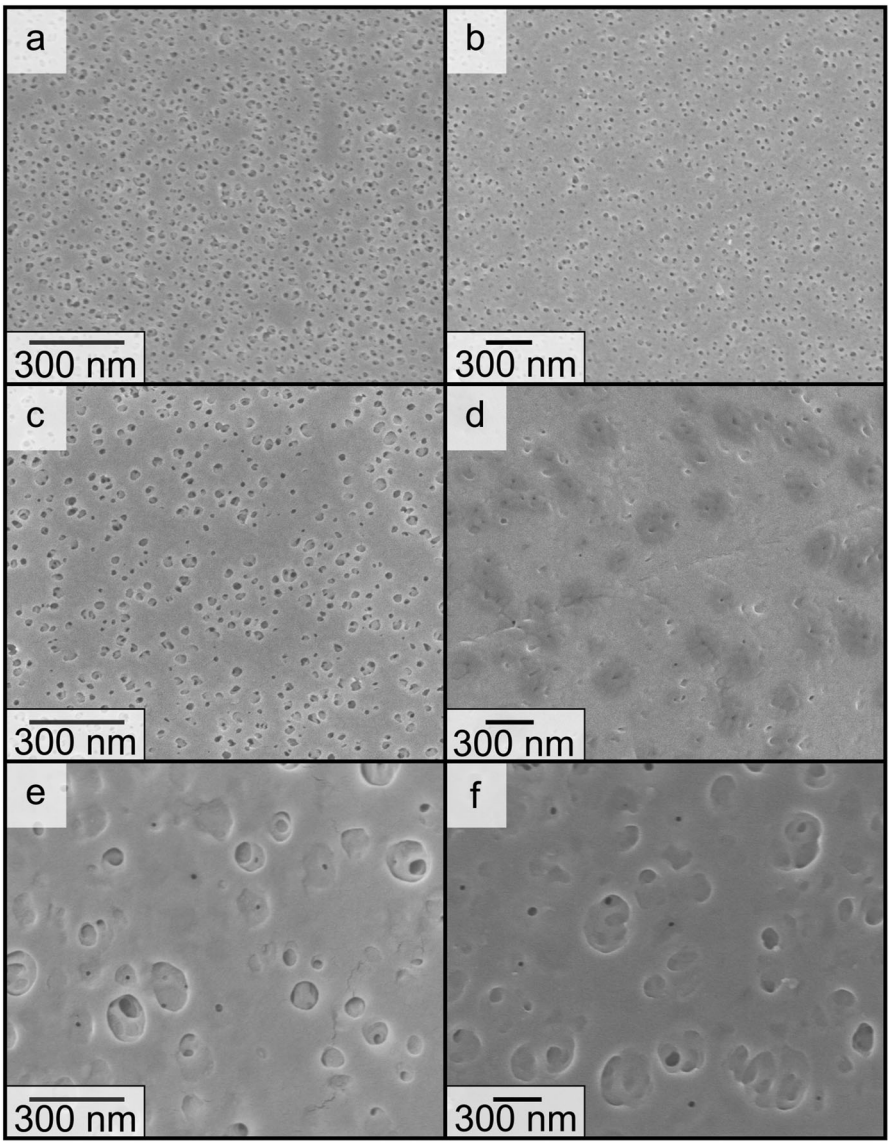

Figure 8. Scanning electron micrographs of the membrane surface from before and after the water permeation measurements at room temperature and 50 °C a) P1 before measurement, featuring a pore size of 22 ± 6 nm b) P1 after measurement, featuring a pore size of 21 ± 4 nm c) P2 before measurement featuring a pore size of 36 ± 8 nm d) P2 after measurement, featuring an irregular surface with some pores still visible e,f) PS_{131}-*b*-$PDEAAm_{42}$ before and after measurement, featuring an irregular surface, with some pores visible.

binary solvent mixture of THF and DMF (2:3 by weight) and block copolymer micelles with a diameter of 45 nm were observed in a TEM micrograph. Based on the Hildebrandt and Hansen parameters of the polymers and solvents, polystyrene micelle cores and a corona of PDEAAm were expected. Ultrafiltration membranes from all three polymers were fabricated using the NIPS procedure. The first tests found a better pore formation at elevated temperatures of the precipitation bath, which was explained by the LCST behavior of the PDEAAm block. Only the polymers PS_{70}-*b*-$PDEAAm_{17}$ and PS_{125}-*b*-$PDEAAm_{43}$ showed a typical membrane surface for the NIPS process. The surface of the membrane of polymer PS_{131}-*b*-$PDEAAm_{42}$ was denser with larger, ill-defined pores. The thermo-responsive behavior of these membranes was investigated using water permeance measurements in a dead-end filtration cell at 1 bar trans-membrane pressure. An up to 23-fold increase in water permeation at 50 °C compared to room temperature was found, which was explained by the PDEAAm chain collapse when crossing the LCST. Differences between the membranes were correlated to the different pore sizes, determined via SEM images. Subsequent measurement of the water permeation at room temperature showed the reversibility of the thermal switching of the membrane for polymers PS_{70}-*b*-$PDEAAm_{17}$ and PS_{131}-*b*-$PDEAAm_{42}$. In contrast, the membrane of polymer PS_{125}-*b*-$PDEAAm_{43}$ was damaged during the experiment. The larger pore size and increased porosity of this membrane sample explained this observation. The addressability of the PDEAAm chains throughout the membrane was shown in a permeance

 © 2023 The Authors. Macromolecular Materials and Engineering published by Wiley-VCH GmbH

14392054, 2023, 11, Downloaded from https://onlinelibrary.wiley.com/doi/10.1002/mame.202300113 by Universitaet Des Saarlandes, Wiley Online Library on [31/01/2024]. See the Terms and Conditions (https://onlinelibrary.wiley.com/terms-and-conditions) on Wiley Online Library for rules of use; OA articles are governed by the applicable Creative Commons License

measurement over a more extended time by comparing the decrease in permeance between room temperature and 50 °C. This new membrane system could find valuable applications in the bio-medicinal separation sector, as the thermo-responsive segment features excellent bio compatibility and the LCST is close to human body temperature. Furthermore, this thermo-responsive membrane could be combined with other external triggers such as pH, redox or light in order to gain additional switchable membrane features for novel applications and separation capabilities.[46–48]

4. Experimental Section

Materials: All chemicals were purchased from Sigma-Aldrich (St. Louis, MO, USA), Fisher Scientific (Hampton, NH, USA), Th. Geyer (Renningen, Germany), TCI (Tokyo, Japan), Deutero (Kastellaun, Germany) and used as received unless otherwise stated. For anionic polymerization THF was treated with 1,1 diphenylethylene (DPE) and *n*-butyllithium (*n*-BuLi). Styrene (S) and *N*,*N*-diethyl acrylamide (DEAAm) were dried by stirring over calcium hydride (CaH_2) followed by cryo transfer to concentrated di *n*-butylmagnesium (0.5 M solution in heptane) or rather trioctylaluminium (25 wt.% in hexane) for DEAAm. After final transfer reagents were stored in a nitrogen-filled glovebox at −18 °C. Anionic polymerizations were carried out under a nitrogen atmosphere in a glovebox equipped with a Coldwell apparatus.

Characterization: Standard size-exclusion chromatography (SEC) in THF was performed with a PSS SECcurity2 system composed of a 1260 IsoPump G7110B (Agilent Technologies, Santa Clara, CA, USA), a 1260 VW-detector G7162A at 270 nm (Agilent) and a 1260 RI-detector G7114A at 30 °C (Agilent), with THF (HPLC grade) as mobile phase (flow rate 1 mL min^{-1}) on a SDV column set (SDV 10^3, SDV 10^5, and SDV 10^6) from PSS (Polymer Standard Service, Mainz, Germany). Calibration was carried out using PS standards (from PSS). SEC in DMF (HPLC grade) was performed with a Waters (Milford, MA, USA) system composed of a 515 HPLC Pump, a 2487 UV-detector at 260 nm and a 2410 RI-detector at 40 °C, with DMF (1 g L^{-1} LiBr) as mobile phase (flow rate 1 mL min^{-1}) on a GRAM column set (GRAM 30, GRAM 1000, and GRAM 1000) from PSS (Polymer Standard Service, Mainz, Germany) at 60 °C. Calibration was carried out using PMMA standards. For data acquisition and evaluation of the measurements, PSS WinGPC UniChrom 8.2 was used.

Nuclear magnetic resonance (NMR) spectra were recorded on a Bruker Avance II 400 spectrometer (Bruker Co, Billerica, MA, USA) with a 9.4 T Ultrashield Plus Magnet, a BBFO probe, and referenced by using the solvent signals. For processing and evaluation of the sprectra MestReNova 14.2.0 (MestReLab Research S.L., Santiago de Compostela, Spain) was used.

Differential scanning calorimetry (DSC) was carried out using a Netzsch DSC 214 Polyma in aluminum crucibles with a heating rate of 10 K min^{-1} and nitrogen as both protective and purge gas in flow rates of 60 and 40 mL min^{-1}, respectively. DSC data were evaluated using NETZSCH Proteus Thermal Analysis 8.0.1.

Ultrathin sections (40 nm) were prepared with an ultramicrotome (Reichert Ultracut by Leica Microsystems, Wetzlar, Germany) and placed on a copper grid.

TEM Images were obtained using a JEOL JEM-2100 LaB_6 electron microscope (JEOL Ltd. Tokyo, Japan) with 200 kV acceleration voltage; 0.14 nm line resolution and a Gatan Orius SC1000 camera (Gatan Inc. Pleasanton, CA, USA) in the brightfield mode.

Staining was a commonly used method for TEM sample preparation and analysis of BCP morphologies in the bulk state. For this purpose, the staining agent was added via vapor deposition – and therefore very low concentrations – to the thin slices of the BCP films. A change in the morphology was not expected, but results obtained from TEM measurements should be compared to other techniques (SAXS, AFM, ...) to verify observed morphologies.[49–51]

Table 4. Exact contents of the NIPS solutions for the different polymer solutions.

Component	PS_{70}-*b*-$PDEAAm_{17}$	PS_{125}-*b*-$PDEAAm_{43}$	PS_{131}-*b*-$PDEAAm_{42}$
Polymer [g]	0.592	0.490	0.489
THF [g]	0.526	0.562	0563
DMF [g]	0.790	0.830	0829
solid content [%]	31.0	26.0	26.0

Scanning electron microscopy (SEM) was carried out on a Zeiss Sigma VP device (GeminiSEM 500) using the software SmartSEM Version 6.07. The samples were mounted on an aluminum stud using adhesive carbon pad and sputter-coated with ≈6 nm platinum using an Automatic Turbo Coater PLASMATOOL 125 SIN 2020_131 from Ingenieurbüro Peter Liebscher. High-resolution micrographs were collected via in-lens detector with acceleration voltages between 1 and 3 kV in high-current mode, 20 µm aperture.

Small-Angle X-ray Scattering (SAXS) experiments were performed using a Xeuss 2.0 instrument (Xenocs, Grenoble, France). The X-ray beam of a copper K_α source (wavelength $\lambda = 0.154$ Å) was focused on the sample with a spot size of 0.25 mm^2. Measurements were performed at a sample-detector distance of ≈2.5 m, calibrated using a silver behenate standard. This resulted in an accessible momentum transfer range of $0.005 < q < 0.23$ $Å^{-1}$, with $q = 4\pi \times \sin(\theta/2)/\lambda$ and θ the scattering angle. The data were azimuthally averaged to obtain $I(q)$. The samples were placed directly in the beam, without the need of using a sample container. The acquisition time for each sample was 1 h.

Synthesis: *Exemplary Synthesis of PS_{70}-b-$PDEAAm_{17}$*

In a nitrogen-filled glovebox 3.30 mL styrene (3.00 g; 28.8 mmol; 800 eq) was dissolved in ≈80 mL of freshly distilled THF. After cooling to −78 °C, 25.7 µL *s*-butyllithium (1.4 M; 36.0 µmol; 1.00 eq) was added quickly to initiate the polymerization. After 1.5 h a sample of the yellow solution was taken, terminated by the addition of degassed MeOH and precipitated. 13.0 µL 1,1-diphenylethylene (13.3 mg; 73.8 µmol; 2.05 eq) were added and the red solution was kept at room temperature for 0.5 h. After cooling to 0 °C, 0.35 mL triethyl borane (1.0 M; 350 µmol; 9.72 eq) and 1.00 mL *N*,*N*-diethyl acrylamide (0.924 g; 7.27 mmol; 202 eq). After a reaction time of 14 h the polymerization was terminated by addition of degassed MeOH. The polymer was precipitated in hexane (synthetic grade) and dried in vacuo at 40 °C. The analytical data for each polymer is presented in Table 1.

^{1}H-NMR (400 MHz; $CDCl_3$; δ in ppm): 7.2–6.2 (br, 5H, ar); 3.6–3.0 (br, 4H, $N(CH_2\text{-}CH_3)_2$); 2.2–0.6 (alkyl).

Bulk Morphologies: The polymers were dissolved in chloroform (p.a.) to examine the bulk morphology of the block copolymers. After slow solvent evaporation, the polymer film was dried in vacuo at 40 °C over night. Finally, the polymer was temperature annealed at 130 °C under a nitrogen atmosphere for at least 4 days. Ultrathin sections (40 nm) were prepared via ultramicrotomy and the resulting films were vapor stained with iodine (>99.5 %) for 3 h or ruthenium oxide (0.5 % in H_2O) for 5 min. For a higher stability, the thin sections were carbon coated. Images of the bulk morphologies were obtained by TEM.

NIPS Process: An appropriate amount of Polymer PS-*b*-PDEAAm was dissolved in a mixture of THF and DMF (2:3 by weight) aiming for a weight fraction of 25%. This polymer solution was cast via a doctor blade with a gap width of 200 µm on a polyester nonwoven support and after 10 s, or 15 s precipitated in a water bath. The water bath was temperature controlled on either room temperature (22 °C) or 40 °C. In **Table 4** the exact measurements are given.

Water-Permeation Measurements: The water permeance measurements were carried out in a dead-end flow cell with a volume of 400 mL and a membrane diameter of 1 cm. Fresh water was supplied by a pressure pot from Sartorius AG, type SM 17 530, whereby the pressure was generated from nitrogen gas.

 © 2023 The Authors. Macromolecular Materials and Engineering published by Wiley-VCH GmbH

14392054, 2023, 11, Downloaded from https://onlinelibrary.wiley.com/doi/10.1002/mame.202300113 by Universitaet Des Saarlandes, Wiley Online Library on [31/01/2024]. See the Terms and Conditions (https://onlinelibrary.wiley.com/terms-and-conditions) on Wiley Online Library for rules of use; OA articles are governed by the applicable Creative Commons License

The water used was purified by an ELGA CLASSIC UVF water purification system and exhibits a resistance of 20 MΩ cm^{-1}.

Measurements at Room Temperature[52]: The membrane was conditioned for 30 min in water before being placed in the dead-end flow cell. The system was operated at a pressure of 1 bar for 1 h, before three samples were collected in 10 min each. The permeation was calculated from the weight of the water as the mean of the three samples.

Measurements at 50 °C: The membrane was conditioned for 1 h in 50 °C water before being placed in the dead-end flow cell, which in turn was placed in a water bath at 50 °C. The system was operated at a pressure of 1 bar for 1 h, before three samples were collected in 10 min each. The permeation was calculated from the weight of the water.

Measurement of Permeation Diagram: For both temperatures the membrane was conditioned the same way as for the permeation measurements and subsequently placed in the filtration system and further conditioned at the measurement pressure for 1 h. The water permeation was monitored over 2–4 h over appropriate time intervals.

Supporting Information

Supporting Information is available from the Wiley Online Library or from the author.

Acknowledgements

The authors thank Blandine Boßmann for help with SEC, DSC and TGA measurements. M.F., J.P., and M.G. thank for partial financial support in the frame of the cooperation platform iCARE for engineering sciences. This research was supported by the DFG project GA2169/7-1 in association with the DFG-funded consortium (DFG-PAK 962/1).

Open access funding enabled and organized by Projekt DEAL.

Conflict of Interest

The authors declare no conflict of interest.

Data Availability Statement

The data that support the findings of this study are available from the corresponding author upon reasonable request.

Keywords

anionic polymerization, block copolymers, LCST polymers, membranes, self-assembly, stimuli-responsive polymers, ultra-filtration

Received: March 28, 2023
Revised: May 12, 2023
Published online: June 4, 2023

[1] M. A. C. Stuart, W. T. S. Huck, J. Genzer, M. Müller, C. Ober, M. Stamm, G. B. Sukhorukov, I. Szleifer, V. V. Tsukruk, M. Urban, F. Winnik, S. Zauscher, I. Luzinov, S. Minko, *Nat. Mater.* **2010**, *9*, 101.
[2] C. G. Schäfer, M. Gallei, J. T. Zahn, J. Engelhardt, G. P. Hellmann, M. Rehahn, *Chem. Mater.* **2013**, *25*, 2309.
[3] L. Montero De Espinosa, W. Meesorn, D. Moatsou, C. Weder, *Chem. Rev.* **2017**, *117*, 12851.
[4] Z.-Q. Cao, G.-J. Wang, *Chem. Rec.* **2016**, *16*, 1398.
[5] Y. Zhao, L.-P. Lv, S. Jiang, K. Landfester, D. Crespy, *Polym. Chem.* **2015**, *6*, 4197.
[6] P. Schattling, F. D. Jochum, P. Theato, *Polym. Chem.* **2014**, *5*, 25.
[7] X. Huang, H. Mutlu, P. Theato, *Nanoscale* **2020**, *12*, 21316.
[8] J. M. Weissman, H. B. Sunkara, A. S. Tse, S. A. Asher, *Science* **1996**, *274*, 959.
[9] F. A. Plamper, M. Ballauff, A. H. E. Müller, *J. Am. Chem. Soc.* **2007**, *129*, 14538.
[10] F. A. Plamper, M. Ruppel, A. Schmalz, O. Borisov, M. Ballauff, A. H. E. Müller, *Macromolecules* **2007**, *40*, 8361.
[11] S. Kuroyanagi, N. Shimada, S. Fujii, T. Furuta, A. Harada, K. Sakurai, A. Maruyama, *J. Am. Chem. Soc.* **2019**, *141*, 1261.
[12] M. Appold, C. Mari, C. Lederle, J. Elbert, C. Schmidt, I. Ott, B. Stühn, G. Gasser, M. Gallei, *Polym. Chem.* **2017**, *8*, 890.
[13] D. Dutta, W. Ke, L. Xi, W. Yin, M. Zhou, Z. Ge, *Wiley Interdiscip. Rev.: Nanomed. Nanobiotechnol.* **2020**, *12*, e1585.
[14] N. Rapoport, *Prog. Polym. Sci.* **2007**, *32*, 962.
[15] A. Kolberg, C. Wenzel, K. Hackenstrass, R. Schwarzl, C. Rüttiger, T. Hugel, M. Gallei, R. R. Netz, B. N. Balzer, *J. Am. Chem. Soc.* **2019**, *141*, 11603.
[16] S. Frost, M. Ulbricht, *J. Membr. Sci.* **2013**, *448*, 1.
[17] B. P. Tripathi, N. C. Dubey, F. Simon, M. Stamm, *RSC Adv.* **2014**, *4*, 34073.
[18] F. Schacher, M. Ulbricht, A. H. E. Müller, *Adv. Funct. Mater.* **2009**, *19*, 1040.
[19] M. Cetintas, J. De Grooth, A. H. Hofman, H. M. Van Der Kooij, K. Loos, W. M. De Vos, M. Kamperman, *Polym. Chem.* **2017**, *8*, 2235.
[20] J. Cai, S. Zhou, Y. Zhao, A. Xue, Y. Zhang, M. Li, W. Xing, *RSC Adv.* **2016**, *6*, 62186.
[21] M. Heskins, J. E. Guillet, *J.Macromol. Sci.: Part A – Chem.* **1968**, *2*, 1441.
[22] I. Idziak, D. Avoce, D. Lessard, D. Gravel, X. X. Zhu, *Macromolecules* **1999**, *32*, 1260.
[23] Y. Maeda, T. Nakamura, I. Ikeda, *Macromolecules* **2002**, *35*, 10172.
[24] H. Cheng, L. Shen, C. Wu, *Macromolecules* **2006**, *39*, 2325.
[25] M. Panayiotou, R. Freitag, *Polymer* **2005**, *46*, 6777.
[26] J. I. Ngadaonye, L. M. Geever, J. Killion, C. L. Higginbotham, *J. Polym. Res.* **2013**, *20*, 161.
[27] D. Baskaran, *Prog. Polym. Sci.* **2003**, *28*, 521.
[28] C. Zune, R. Jérôme, *Prog. Polym. Sci.* **1999**, *24*, 631.
[29] T. Ishizone, K. Yoshimura, A. Hirao, S. Nakahama, *Macromolecules* **1998**, *31*, 8706.
[30] M. Kobayashi, S. Okuyama, T. Ishizone, S. Nakahama, *Macromolecules* **1999**, *32*, 6466.
[31] X. André, K. Benmohamed, A. V. Yakimansky, G. I. Litvinenko, A. H. E. Müller, *Macromolecules* **2006**, *39*, 2773.
[32] M. Kobayashi, T. Ishizone, S. Nakahama, *Macromolecules* **2000**, *33*, 4411.
[33] L. Vinogradova, L. Fedorova, H.-J. P. Adler, D. Kuckling, D. Seifert, C. B. Tsvetanov, *Macromol. Chem. Phys.* **2005**, *206*, 1126.
[34] J. Brandrup, E. H. Immergut, E. A. Grulke, A. Abe, D. R. Bloch, *Polymer Handbook*, Wiley, New York **1999**.
[35] I. W. Hamley, V. Castelletto, *Prog. Polym. Sci.* **2004**, *29*, 909.
[36] M. W. Matsen, F. S. Bates, *Macromolecules* **1996**, *29*, 1091.
[37] A. F. M. Barton, *Chem. Rev.* **1975**, *75*, 731.
[38] R. Mieczkowski, *Eur. Polym. J.* **1989**, *25*, 1055.
[39] H. Ahmad, *J. Macromol. Sci.: Part A – Chem.* **2006**, *17*, 585.
[40] S. P. Nunes, *Macromolecules* **2016**, *49*, 2905.
[41] G. Luna-Bárcenas, D. G. Gromov, J. C. Meredith, I. C. Sanchez, J. J. De Pablo, K. P. Johnston, *Chem. Phys. Lett.* **1997**, *278*, 302.
[42] T. E. De Oliveira, C. M. Marques, P. A. Netz, *Phys. Chem. Chem. Phys.* **2018**, *20*, 10100.

 © 2023 The Authors. Macromolecular Materials and Engineering published by Wiley-VCH GmbH

14392054, 2023, 11, Downloaded from https://onlinelibrary.wiley.com/doi/10.1002/mame.202300113 by Universitaet Des Saarlandes, Wiley Online Library on [31/01/2024]. See the Terms and Conditions (https://onlinelibrary.wiley.com/terms-and-conditions) on Wiley Online Library for rules of use; OA articles are governed by the applicable Creative Commons License

[43] C. A. Smolders, A. J. Reuvers, R. M. Boom, I. M. Wienk, *J. Membr. Sci.* **1992**, *73*, 259.
[44] M. Gallei, S. Rangou, V. Filiz, K. Buhr, S. Bolmer, C. Abetz, V. Abetz, *Macromol. Chem. Phys.* **2013**, *214*, 1037.
[45] K. M. Persson, V. Gekas, G. Trägårdh, *J. Membr. Sci.* **1995**, *100*, 155.
[46] J. Morsbach, J. Elbert, C. Rüttiger, S. Winzen, H. Frey, M. Gallei, *Macromolecules* **2016**, *49*, 3406.
[47] R. H. Staff, M. Gallei, K. Landfester, D. Crespy, *Macromolecules* **2014**, *47*, 4876.
[48] C. Rüttiger, S. Mehlhase, S. Vowinkel, G. Cherkashinin, N. Liu, C. Dietz, R. W. Stark, M. Biesalski, M. Gallei, *Polymer* **2016**, *98*, 429.
[49] M. Steube, T. Johann, M. Plank, S. Tjaberings, A. H. Gröschel, M. Gallei, H. Frey, A. H. E. Müller, *Macromolecules* **2019**, *52*, 9299.
[50] C. Rüttiger, M. Appold, H. Didzoleit, A. Eils, C. Dietz, R. W. Stark, B. Stühn, M. Gallei, *Macromolecules* **2016**, *49*, 3415.
[51] M. Appold, C. Rüttiger, B. Kuttich, B. Stühn, M. Gallei, *Macromol. Chem. Phys.* **2018**, *219*, 1700187.
[52] J. Gaalken, M. Ulbricht, *J. Polym. Sci.* **2020**, *58*, 2561.

 © 2023 The Authors. Macromolecular Materials and Engineering published by Wiley-VCH GmbH

14392054, 2023, 11, Downloaded from https://onlinelibrary.wiley.com/doi/10.1002/mame.202300113 by Universitaet Des Saarlandes, Wiley Online Library on [31/01/2024]. See the Terms and Conditions (https://onlinelibrary.wiley.com/terms-and-conditions) on Wiley Online Library for rules of use; OA articles are governed by the applicable Creative Commons License